Dalton Transactions

Accepted Manuscript

ROYAL SOCIETY OF CHEMISTRY

www.rsc.org/dalton

Journal Name

RSCPublishing

ARTICLE

Specificity of the Zn^{2+}, Cd^{2+} and Ni^{2+} ion binding sites in the loop domain of the HypA protein

Cite this: DOI: 10.1039/x0xx00000x

Received 00th January 2012,
Accepted 00th January 2012

DOI: 10.1039/x0xx00000x

www.rsc.org/

Paulina Kolkowska,[a] Karolina Krzywoszynska,[a] Slawomir Potocki,[a] Parashurampura Renukaprasanna Chetana,[b] Marta Spodzieja,[c] Sylwia Rodziewicz-Motowidlo[c] and Henryk Kozlowski[a]

The zinc binding loop domain of *Helicobacter pylori's* HypA protein consists of two CXXC motifs with flanking His residues. These motifs bind metal ions and thus they are crucial for the functioning of the whole protein. The N-terminal site, where His is separated from CXXC by Ser residue is more effective in binding Zn^{2+} and Ni^{2+} ions than the C-terminal site, in which His is next to CXXC motif. Studies on various modifications of the peptide sequence within the Ac-ELECKDCSHVFKPNALDYGVCEKCHS-NH_2 loop show the role of the residues in the linker between CXXC motifs and the effect of length of the linker on the stability of the complexes it forms with Zn^{2+}, Cd^{2+} and Ni^{2+} ions. The proline residue in the linker between two CXXC binding sites plays a distinct role in the metal ion binding ability of the loop, lowering the efficacy of metal ion coordination. Deletion of the aliphatic residues from the linker between CXXC motifs remarkably improves the binding efficacy of the loop.

Introduction

Helicobacter pylori is a pathogen, which when found in the human stomach, may lead to the development of gastritis and peptic ulcers and it is also classified as human carcinogen.[1,2] Despite declining of prevalence of this bacterial infection in developed countries, still approximately 80% of the adult population in developing countries is infected by *H. pylori*.[3] Interestingly, the ability of these bacteria to survive in tough, acidic conditions of the human stomach environment is made possible by the presence of nickel dependent enzymes - urease and [NiFe] hydrogenase. Urease increases the acid gastric pH around bacterium cell by catalyzing the hydrolysis of urea to ammonia.[4] The role of the second enzyme is to supply energy to the cell from oxidation of molecular hydrogen.[5] Many accessory proteins are needed for the maturation and activation of those two enzymes, therefore much of the *H. pylori* metal metabolism is focused on the expression and maturation of urease and [NiFe] hydrogenase.[6] These facts show that exploring the homeostasis of metal ions in bacteria is an important and wide field of study and it has lately been frequently reviewed.[7-9] The understanding of the mechanism of the metal homeostasis can open the way to a safe and effective eradication of these microorganisms[10] and it is also very fascinating from the point of view of bioinorganic chemistry.

HypA is one of the accessory protein from *H. pylori*. This metal chaperone, in cooperation with HypB, is involved in nickel incorporation into the [NiFe] hydrogenase. Both proteins bind Ni^{2+} ions and are required for urease activity.[11] Details of the mechanism of their cooperation are still under investigation. Xia and co-workers found that HypA delivers nickel ions into HypB,[12] while other studies have shown a reverse situation, in which HypA is an acceptor of Ni^{2+}.[13]

HypA can form a homodimer and together with HypB - heterodimer.[14] Monomeric HypA consists of two metal binding domains: an N-terminal nickel site and zinc binding domain located in the C-terminal loop. Most probably, Zn^{2+} ions play a structural role in this protein.[15] What is more, the amino acid sequence of HypA from various bacteria contains conserved residues in the metal binding sites. The conserved MHE motif is present in the nickel binding domain, whereas in the zinc site, there are two conserved CXXC motifs.[16,17] Recently, these two domains were extensively studied. Structure determination of HypA from *H. pylori* by NMR revealed that Ni^{2+} is anchored to

His2 and Glu3 from MHE motif and to Asp40. It forms square-planar complex with 4N donors.[16] In contrast, XAS analysis showed a 5 or 6 coordination sphere with N/O donors for the nickel ion.[17] In case of the zinc binding site, data from ^{113}Cd NMR spectroscopy with ^{113}Cd-reconstituted HypA proved tetrahedral coordination to zinc ion by four sulfur atoms from Cys74, Cys77, Cys91 and Cys94 which are in the conserved CXXC motifs.[16] K-edge XAS spectra showed that the zinc site changes upon binding Ni^{2+}. In the apoprotein, it consists of three thiols and one N/O donor ligand.[17] These findings reveal dynamics of zinc binding site, demonstrated in previous work.[14] Further studies, based on the combination of NMR, XAS data and mutagenesis, led to a hypothesis that the zinc binding site is not only sensitive to nickel ion binding, but also to the change of pH. At pH 6.3, which occurs in the interior of the bacterial cell during acid shock, the zinc site undergoes ligand substitutions - $Zn(Cys)_4$ changes to $Zn(His)_2(Cys)_2$. The coordination sphere of Ni^{2+} remains unaffected (5-6 N/O donor ligands), but the stoichiometry of binding to dimeric HypA changes from two nickel ions per dimer to one nickel ion per dimer. These studies provide evidence that there is communication between the nickel and zinc site in HypA. In this model, modification of the zinc binding mode in response to internal pH allows proper delivery of nickel ion to target protein. Moreover, histidine residues flanking the CXXC motifs play an important role in pH sensing.[18]

Another insight into coordination behavior of HypA was given by studies on the Ac-ELECKDCSHVFKPNALDYGVCEKCHS-NH_2 fragment of the loop region from *H. pylori*. The protein fragment contains two CXXC motifs and flanking histidine residues relevant for metal ion binding. Potentiometric, NMR, mass spectrometry and spectroscopic measurements with this peptide have confirmed that cysteine residues are crucial in Zn^{2+} binding. However, histidine residues are involved in Zn^{2+} coordination in lower pH, whereas the $Zn(Cys)_4$ complex is formed above pH 7.[19]

Taking into account the above findings, we decided to explore the details of the coordination behavior of the HypA loop towards Zn^{2+}, Cd^{2+} and Ni^{2+} ions. First our studies were focused on the flanking histidine residues and their role in HypA loop. Shorter peptides comprising the N-terminal motif, with His separated from Cys pair by Ser residue (peptide ELE), with the C-terminal motif, where His is next to CXXC (peptide DYG) and their analogues lacking histidine residues (ELES and DYGS), were studied to elucidate the role of His residue in metal ion coordination in both binding domains.

The effect of the linker length and amino acid residue composition on the thermodynamic stability of the metal ions complexes were also studied. To understand the role of the proline residue, which usually has a strong impact on structural features of the peptide,[20] it was mutated to Ala (peptide HypA1). Subsequently, we made a deletion of some residues from the linker, hydrophobic residues and His, which caused decreasing of the distance between CXXC motifs (peptides HypA2, HypA3 and HypA4). Sequences of all investigated peptides are listed in Table 1.

Table 1 Sequences of the studied peptides and comparison to the HypA WT.

Name	Sequences	Modification	Length of the linker
HypA WT	Ac-ELECKDCSHVFKPNALDYGVCEKCHS-NH_2	-	CXXC-$(X)_5$-P-$(X)_7$-CXXC
HypA1	Ac-ELECKDCSHVFKANALDYGVCEKCHS-NH_2	P-A	CXXC-$(X)_5$-A-$(X)_7$-CXXC
HypA2	Ac-ELECKDCSHKPNDYGVCEKCHS-NH_2	$_{80}$VF $_{85}$AL	CXXC-$(X)_3$-P-$(X)_5$-CXXC
HypA3	Ac-ELECKDCSHKPNDYCEKCHS-NH_2	$_{80}$VF $_{85}$ AL $_{89}$GV	CXXC-$(X)_3$-P-$(X)_3$-CXXC
HypA4	Ac-ELECKDCKPNCEKCHS-NH_2	$_{78}$SHVF $_{85}$ALDYGV	CXXC-X-P-X-CXXC
ELE	Ac-ELECKDCSHV-NH_2	-	-
DYG	Ac-DYGVCEKCHS-NH_2	-	-
ELES	Ac-ELECKDCSSV-NH_2	-	-
DYGS	Ac-DYGVCEKCSS-NH_2	-	-

Experimental

Peptide synthesis and purification

Peptides HypA1-HypA4, DYG and ELE were purchased from Selleckchem (USA). Peptides ELES and DYGS were synthesized by solid phase peptide synthesis (SPPS) with a semiautomated peptide synthesizer Millipore 9050 Plus PepSynthesizer, (Millipore Corporation, Burlington, VT,USA) using general conditions of solid-phase synthesis.[21,22] Synthesis were performed on a TentaGel R RAM resin (0.19 mmol/g), using 9-fluorenylmethoxycarbonyl/tert-butyl (Fmoc/tBu) chemistry with the following side chain protected amino acid derivatives: Fmoc-Glu(OtBu)-OH, Fmoc-Leu-OH, Fmoc-

Cys(Trt)-OH, Fmoc-Lys(Boc)-OH, Fmoc-Asp(OtBu)-OH, Fmoc-Ser(tBu)-OH, Fmoc-Val-OH, Fmoc-Tyr(tBu)-OH and Fmoc-Gly-OH. Acetylation of the N-terminal amino group of the peptides were performed using 1-acetylimidazole (1.10 g/1g of resin at room temperature for 24 h). The peptides were cleaved from the resin using a mixture of TFA, fenol, deionized water and triethylsilane (88:5:5:2 v/v/v/v) (10 ml/1 g of resin at room temperature for 2 h). After filtration of the exhausted resin, the solvent was concentrated in vacuo, and the residue was triturated with diethyl ether. The precipitated peptides were centrifuged for 15 min, followed by decantation of the ether phase from the crude peptides. This washing/decantation process was repeated three times. After evaporation of diethyl ether, the peptides were dissolved in H_2O and lyophilized.

The crude peptides were purified by semi-preparative RP-HPLC on a Kromasil C8 column (250 mm, 20 mm, 5 μm) with 80 % acetonitrile in aqueous 0.08 % TFA (solvent B) and 0.1 % TFA in MilliQ water (solvent A) as mobile phases. A linear gradient from 5% B to 35% B in A in 120 min was used. Purification was monitored by UV absorption at a wavelength of 222 nm. Purity of the peptides was checked using analytical RP-HPLC (Kromasil C8 column, 250 mm, 4.6 mm, 5 μm) and gradient from 0% to 100% B in A and mass spectrometer ESI IT TOF (Shimadzu, Shimpol, Warsaw, Poland).

Potentiometric measurements

Stability constants for the proton, Zn^{2+}, Ni^{2+} and Cd^{2+} complexes were calculated from pH-metric titration curves carried out under argon atmosphere (to avoid oxidation of cysteine residues) in the pH range 2.5-11 at 298 K. Measurements were performed in 0.1 M KCl using a total volume of 1.5-2.5 ml on a MOLSPIN pH-meter system using a Russel CMAW 711 semi-combined electrode and on an automatic titration system Titrando 809 (Metrohm) with a combined glass electrode (Mettler Toledo InLab Semi-Micro), both electrodes were calibrated in proton concentrations using HCl.[23] Alkali (NaOH) was added from a 0.250 ml micrometer syringe, which was calibrated by weight titration and the titration of standard materials. The Gran method was used to determine exact concentration and purification of the ligand solutions.[24] The ligands concentrations were 1×10^{-3} M and the ligands to metals molar ratios were 3:1, 2:1 and 1:0.9. The SUPERQUAD and HYPERQUD 2006 programs were used for the stability constant calculations.[25,26] Standard deviations were computed by HYPERQUAD 2006 and refer to random errors only. All solutions before measurements were deaerated.

UV-VIS and CD measurements

The absorption spectra were recorded on a Cary 300 Bio spectrophotometer, and circular dichroism (CD) spectra were recorded on Jasco J715 spectropolarimeter in the 800-230 nm range at 298 K using a total volume of 2 ml. The concentration of the ligands were 1×10^{-3} M for nickel complexes and 1×10^{-4} M for cadmium complexes, and the ligands to metals molar ratios were 3:1, 2:1 and 1:0.9. All solutions before measurements were deaerated and carried out under argon atmosphere. The values of ε and Δε (i.e. ε_l - ε_r) were calculated at the maximum concentration of the respective species obtained from potentiometric data.

Mass spectrometric measurements

High-resolution mass spectra were obtained on a BrukerQ-FTMS and a Bruker micrOTOF-Q spectrometers (Bruker Daltonik, Bremen, Germany), equipped with an Apollo II electrospray ionization source with an ion funnel. The mass spectrometers were operated both in the positive and negative ion mode. The instrumental parameters were as follows: scan range m/z 400–1600, dry gas–nitrogen, temperature 170°C, ion energy 5eV. Capillary voltage was optimized to the highest S/N ratio and it was 4500 V. The small changes of voltage (± 500V) did not significantly affect the optimized spectra. The sample (metal:ligand in a 1:2 stoichiometry, [ligand] = 1×10^{-4} M) was prepared in 1:1 MeOH-H_2O mixture at pH 7.4. Variation of the solvent composition down to 5% of MeOH did not change the species composition. The sample was infused at a flow rate of 3 μL/min. The instrument was calibrated externally with the Tunemix™ mixture (Bruker Daltonik, Germany) in quadratic regression mode. Data were processed by using the Bruker Compass DataAnalysis 4.0 program. The mass accuracy for the calibration was better than 5 ppm, enabling together with the true isotopic pattern (using SigmaFit) an unambiguous confirmation of the elemental composition of the obtained complex.

NMR measurements

NMR spectra were recorded at 14.1 T on a Bruker Avance III 600 MHz. Temperatures were controlled with an accuracy of ±0.1 K. All samples were prepared in a 90% H_2O and 10% D_2O (99.95% from Merck) mixture. Proton resonance assignment was accomplished by 2D ^1H–^1H total correlation spectroscopy (TOCSY) and nuclear Overhauser effect spectroscopy (NOESY). Experiments were carried out with standard pulse sequences and spectral processing was performed using Bruker TOPSPIN 2.1. Samples of complexes were prepared by adding metal ion to an acidic solution of a ligand (pH 3.5). and the pH was then increased to a higher value.

Results and discussion

Protonation constants

Protonation constants for studied peptides and possible assignments to the particular functions are presented in Tables 2-10. Charges of the species were omitted for simplicity in the whole article.

All peptides were protected at the C and N termini, thus all of the ligands protonation constants can be assigned to the deprotonation of the side chain groups.

Ac-ELECKDCSHV-NH_2 peptide (ELE) behaves as H_7L acid, its analogue Ac-ELECKDCSSV-NH_2 (ELES) exhibits six

Table 2 Potentiometric and spectroscopic data for proton, Zn^{2+}, Cd^{2+} and Ni^{2+} complexes of the ELE peptide.

			UV-Vis		CD	
Species	**log *β***	**p*K***	**λ/nm**	**ε/M^{-1} cm^{-1}**	**λ/nm**	**Δε/M^{-1} cm^{-1}**
HL	10.98 (1)	10.98 K				
H_2L	20.63 (1)	9.65 C				
H_3L	29.33 (1)	8.70 C				
H_4L	36.27 (1)	6.94 H				
H_5L	41.21 (2)	4.94 E				
H_6L	45.30 (2)	4.09 E				
H_7L	48.67 (2)	3.37 D				
Zn^{2+} complexes L:M 1:0.9						
ZnH_3L	34.28 (3)					
ZnH_2L	29.27 (1)	5.01				
ZnHL	23.02 (2)	6.25				
ZnL	12.32 (3)	10.70				
$ZnH_{-1}L$	1.34 (3)	10.98				
Zn^{2+} complexes L:M 2:1						
ZnH_3L	34.79 (2)					
ZnH_2L	29.58 (2)	5.21				
ZnHL	23.60 (4)	5.97				
ZnH_4L_2	56.23 (6)					
ZnH_3L_2	48.77 (4)	7.47				
ZnH_2L_2	39.75 (4)	9.01				
ZnL_2	18.37 (4)					
Cd^{2+} complexes L:M 1:0.9						
CdH_3L	35.94 (1)		242	3790		
CdH_2L	30.73 (2)	5.21	242	6670		
CdHL	24.48 (3)	6.25	242	12450		
CdL	13.66 (3)	10.82	242	12450		
Cd^{2+} complexes L:M 2:1						
CdH_3L	36.17 (1)		240	4240		
CdH_2L	30.89 (2)	5.28	240	12190		
CdHL	25.05 (2)	5.84	240	12980		
CdH_3L_2	51.20 (2)		240	14060		
CdH_2L_2	42.70 (3)	8.50	242	22620		
CdL_2	21.29 (3)		242	25670		
Ni^{2+} complexes L:M 1:0.9, 2:1						
NiHL	20.61 (1)		255	8025	248	1.17
			292	4995	269	1.96
			335	1280	303	-0.44
			389	640	364	-0.18
					447	0.73
					559	0.18
NiL	11.38 (4)	9.23	255	11010	239	2.88
			290	5660	271	3.50
			339	950	305	-0.93
			394	490	437	0.80
					512	-0.52
					587	0.30
$NiH_{-1}L$	1.39 (3)	9.99	258	11610	238	4.25
			292	5110	271	3.75
			451	175	303	-1.13
					437	0.80
					512	-0.45
					587	0.32
$NiH_{-2}L$	-9.11 (3)	10.50	258	11820	239	3.75
			292	5100	271	3.79
			450	170	304	-1.09
					439	0.80
					512	-0.41
					587	0.30

Table 3 Potentiometric and spectroscopic data for proton, Zn^{2+}, Cd^{2+} and Ni^{2+} complexes of the ELES peptide.

			UV-VIS		CD	
Species	**log *β***	**p*K***	**λ/nm**	**ε/M^{-1} cm^{-1}**	**λ/nm**	**Δε/M^{-1} cm^{-1}**
HL	11.02 (1)	11.02 K				
H_2L	20.55 (1)	9.53 C				
H_3L	28.80 (1)	8.25 C				
H_4L	33.57 (1)	4.77 E				
H_5L	37.68 (1)	4.11 E				
H_6L	41.33 (1)	3.65 D				
Zn^{2+} complexes L:M 1:0.9						
ZnH_2L	26.61 (3)					
ZnHL	21.56 (1)	5.05				
ZnL	11.78 (2)	9.78				
$ZnH_{-1}L$	1.13 (2)	10.65				
Zn^{2+} complexes L:M 2:1						
ZnH_3L	32.31 (3)					
ZnH_2L	27.45 (3)	4.86				
ZnH_4L_2	54.51 (2)					
ZnH_3L_2	47.54 (5)	6.97				
ZnH_2L_2	39.57 (5)	7.97				
ZnL_2	18.12 (5)					
Cd^{2+} complexes L:M 1:0.9						
CdH_2L	28.03 (1)		242	4420		
CdHL	22.53 (2)	5.50	242	10680		
CdL	11.88 (2)	10.65	242	11780		
Cd^{2+} complexes L:M 2:1						
CdH_3L	32.12 (6)		minor			
CdH_2L	28.05 (2)	4.07	240	5200		
CdH_4L_2	55.30 (3)		240	10130		
CdH_3L_2	49.08 (4)	6.22	240	18860		
CdH_2L_2	42.38 (3)	6.70	240	31820		
CdL_2	20.77 (4)		240	35300		
Ni^{2+} complexes L:M 1:0.9, 2:1						
NiLH	18.22 (3)		271	6660	252	0.53
			338	1470	260	-0.27
			336	1230	283	4.60
			550	210	331	0.57
					349 sh	0.42
					381	-1.24
					475sh	-1.03
					576	1.15
$NiLH_{-1}$	-4.36 (4)		270	7770	251	1.41
			366	1230	283	5.67
			451	340	324	1.09
			550	215	353	0.59
					387	-1.15
					452sh	-1.88
					578	1.91

protonation constants, while for Ac-DYGVCEKCHS-NH_2 (DYG) peptide six of seven protonation constants were evaluated. For Ac-DYGVCEKCSS-NH_2 (DYGS), where histidine residue was replaced by serine residue, six protonation constants were calculated.

Ligands Ac-ELECKDCSHVFKPNALDYGVCEKCHS-NH_2 (HypA WT), Ac-ELECKDCSHVFKANALDYGVCEKCHS-NH_2 (HypA1), Ac-ELECKDCSHKPNDYGVCEKCHS-NH_2 (HypA2) and Ac-ELECKDCSHKPNDYCEKCHS-NH_2

(HypA4) have potentially fifteen protonation constants. Only eleven of them were detected by the potentiometric measurements; the remaining three are beyond the detection range of the electrode . We were able to detect ten of twelve

Table 4 Potentiometric and spectroscopic data for proton, Zn^{2+}, Cd^{2+} and Ni^{2+} complexes of the DYG peptide.

			UV-Vis		CD	
Species	**log *β***	**p*K***	**λ/nm**	**ε/M^{-1} cm^{-1}**	**λ/nm**	**Δε/M^{-1} cm^{-1}**
HL	10.21 (1)	10.21 Y				
H_2L	19.51 (1)	9.30 C				
H_3L	27.85 (1)	8.34 C				
H_4L	34.40 (1)	6.55 H				
H_5L	38.87 (1)	4.47 E				
H_6L	42.43 (1)	3.56 D				
Zn^{2+} complexes L:M 1:0.9						
ZnH_2L	27.43 (1)					
ZnHL	21.20 (2)	6.23				
ZnL	12.48 (3)	8.72				
$ZnH_{-1}L$	2.29 (3)	10.19				
Zn^{2+} complexes L:M 2:1						
ZnH_2L	27.15 (2)					
ZnH_5L_2	59.57 (1)					
ZnH_4L_2	53.27 (2)	6.30				
ZnH_3L_2	45.68 (2)	7.59				
ZnH_2L_2	36.28 (2)	9.40				
$ZnHL_2$	26.23 (3)	10.05				
ZnL_2	16.12 (2)	10.11				
Cd^{2+} complexes L:M 1:0.9						
CdH_3L	33.38 (3)		250	2260		
CdH_2L	29.10 (1)	4.28	250	5870		
CdHL	23.50 (3)	5.60	250	8890		
CdL	13.30 (3)	10.20	250	17520		
Cd^{2+} complexes L:M 2:1						
CdH_3L	33.12 (5)		minor			
CdH_2L	28.92 (2)	4.20	247	6065		
CdHL	23.75 (3)	5.17	247	6640		
CdH_4L_2	55.68 (4)		247	16305		
CdH_3L_2	49.21(3)	6.47	247	17770		
CdH_2L_2	40.81 (4)	8.40	247	19200		
CdL_2	20.85 (4)		247	24900		
Ni^{2+} complexes L:M 1:0.9, 2:1						
NiH_2L	24.74 (5)		minor			
NiHL	18.75 (2)	5.99	275	9325	256	2.44
			312	5270	283	4.81
			350	3340	322	5.29
			517	610	370	-7.23
					507	4.46
					660	-0.26
NiL	9.32 (3)	9.43	244	18110	254	1.90
			275	11340	283	4.52
			350	2250	323	4.07
			517	450	370	-5.48
					503	2.92
$NiH_{-2}L$	-11.02 (2)		238	25640	242	2.27
			350	825	280	4.05
			517	220	313	1.32
					388	-1.43
					450	0.76
					531	-0.72

Table 5 Potentiometric and spectroscopic data for proton, Zn^{2+}, Cd^{2+} and Ni^{2+} complexes of the DYGS peptide.

			UV-Vis		CD	
Species	**log *β***	**p*K***	**λ/nm**	**ε/M^{-1} cm^{-1}**	**λ/nm**	**Δε/M^{-1} cm^{-1}**
HL	10.62 (1)	10.62 K				
H_2L	20.64 (1)	10.02 Y				
H_3L	29.76 (1)	9.12 C				
H_4L	37.83 (1)	8.07 C				
H_5L	42.38 (1)	4.55 E				
H_6L	45.83 (1)	3.45 D				
Zn^{2+} complexes L:M 1:0.9						
ZnH_3L	35.46 (4)					
ZnH_2L	30.64 (1)	4.82				
ZnHL	21.52 (2)	9.12				
ZnL	10.91 (3)	10.61				
$ZnH_{-1}L$	-0.33 (6)	11.24				
Zn^{2+} complexes L:M 2:1						
ZnH_2L	31.01 (2)					
ZnH_4L_2	60.40 (3)					
ZnH_2L_2	40.48 (4)					
ZnL_2	18.18 (4)					
Cd^{2+} complexes L:M 1:0.9						
CdH_2L	32.38 (2)		242	10090		
CdHL	22.18 (5)	10.20	238	18720		
CdL	11.33 (4)	10.85	235	24665		
Cd^{2+} complexes L:M 2:1						
CdH_2L	32.64 (2)		242	6260		
CdH_4L_2	62.86 (4)		242	20520		
CdH_3L_2	52.66 (5)	10.20	242	33960		
CdL_2	20.24 (5)		239	46710		
Ni^{2+} complexes L:M 1:0.9, 2:1						
NiH_2L	28.36 (1)		222	15260	265	-5.50
			275	2890	337	2.94
			302	1980	402	-1.41
			345	1080	496	-0.10
					560	0.49
NiHL	19.12 (4)	9.24	268	10570	265	-5.50
			272	7190	287	0.93
			372	1385	334	2.43
			455	520	397	-1.80
					442	0.56
					500	-0.87
					583	0.63
NiL	9.81 (3)	9.31	272	11940	267	-4.30
			372	1220	285	1.83
			455	450	298	0.41
					335	2.30
					390	-2.00
					443	1.00
					508	-1.00
					592	0.59
$NiH_{-2}L$	-11.66 (3)		272	12190	264	-2.10
			372	1160	285	2.85
			455	420	333	1.36
					383	-1.74
					441	0.97
					510	-1.10
					594	0.30

protonation constants of Ac-ELECKDCKPNCEKCHS-NH_2 (HypA4) peptide.

Metal complexes

Mass spectrometric measurements reveal presence of Zn^{2+}, Ni^{2+} and Cd^{2+} complexes with investigated peptides. In the case of the long sequences (HypA WT, HypA1, HypA2, HypA3 and HypA4) only equimolar species were found. In contrast, shorter peptides ELE, ELES, DYG and DYGS form both equimolar and bis-complexes with Zn^{2+} and Cd^{2+} depending on ligand to metal molar ratio. Shorter peptides do not form bis-complexes with Ni^{2+}. In ESI-MS data, both m/z ratios and isotopic patterns are identical for all experimental and simulated signals (Fig. S1-S7). Potentiometric and spectroscopic data for the studied complexes are collected in Tables 2-10 and in the supplementary data (Fig. S1-S34).

The role of the flanking histidine residues in CXXC motifs in binding ability of HypA loop

Zn^{2+} complexes with ELE, ELES, DYG and DYGS peptides

Short peptides ELE and DYG, and their analogues without the histidine residue - ELES and DYGS - form both equimolar and bis-complexes with Zn^{2+} (Tables 2-5; Fig. S8-S9). According to calculations based on potentiometric data for the Zn^{2+}-ELE system five equimolar complexes are formed (Table 2). The first major species, ZnH_2L, which dominates at pH above 4 (Fig. S8), involves thiol and imidazole nitrogen donors in the binding. In the ZnHL species (present at pH above 5) the mode of the coordination is {2S, N_{im}} with the second thiol coordinated to Zn^{2+}. This binding mode is strongly supported by the ^{1}H-^{1}H TOCSY spectra at pH 7.4. Hα–Hβ correlations from cysteine residues and Hα–Hβ correlations from aromatic protons of histidine residue are shifted compared to the spectra of the free ligand at the same pH (Fig. 1). The next two deprotonation (ZnL and $ZnLH_{-1}$ complexes) come from a water molecule bound to the metal ion and from the side chain of lysine, which does not participate in binding.

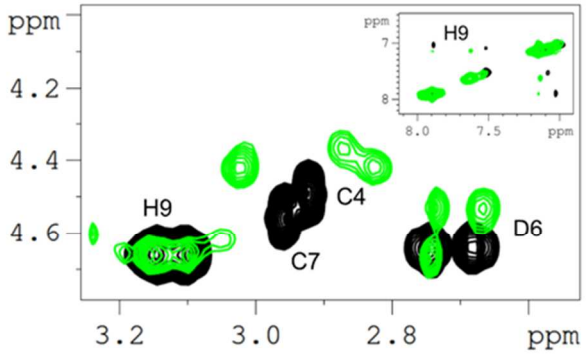

Fig. 1 Selected aliphatic and aromatic regions of the ^{1}H–^{1}H TOCSY spectra of ELE at 1×10^{-3} M, pH 7.4 and T 303 K in the absence (black contours) and in the presence (green contours) of 0.6 Zn^{2+} equivalents.

In the case of equimolar complexes of ELES, two thiols from cysteine residues are bound to Zn^{2+}, which is confirmed by potentiometric data (Table 3). The pK value corresponding to the loss of the thiol protons in the zinc species (5.05) is significantly lower compared to free ligand (9.53). The comparison of the binding ability of both peptides on the competition plot (Fig. 2) clearly indicate that the ELE ligand is more efficient in binding zinc than the ELES peptide. This can be explained by the involvement of histidine residue in the binding of Zn^{2+} in ELE.

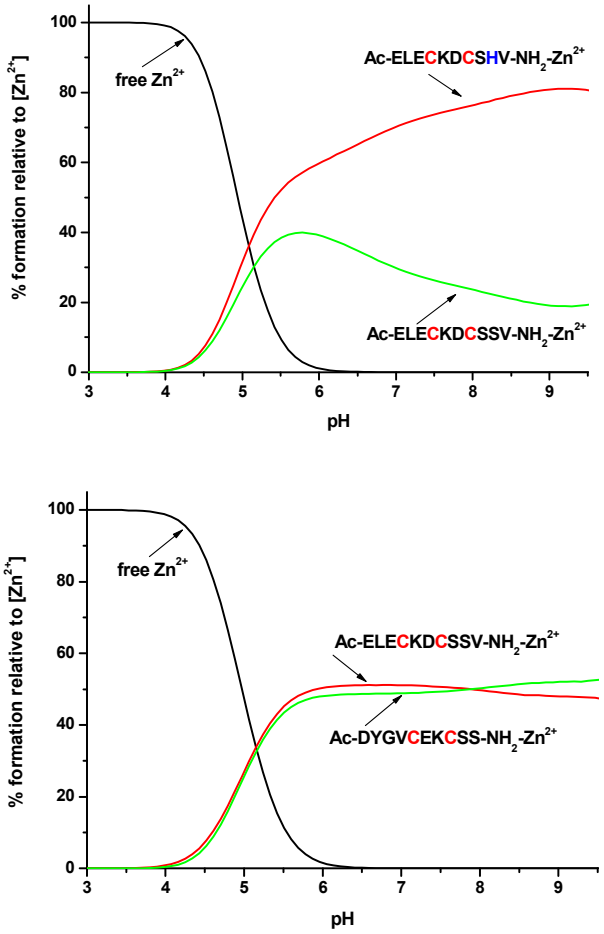

Fig. 2 Competition plots of Zn^{2+} complexes with ELE and ELES (1 : 1 : 1 molar ratio).(top) and with ELES and DYGS (1 : 1 : 1 molar ratio) (bottom).

Peptides DYG and DYGS behave similarly to peptides described above (Tables 4-5; Fig. S8-S9) . The binding mode of complexes with Zn^{2+} is {2S, N_{im}} for the first one (ZnHL) detected at low pH and {2S} for the latter one (ZnH_2L), which is confirmed by potentiometric and NMR data. In ^{1}H-^{1}H TOCSY spectra at pH 7.4, Hα–Hβ correlations from cysteine residues and correlations from aromatic protons of the histidine residue are vanished compared to the spectra of free ligand at the same pH (Fig. S10). Also in this case, the peptide with His residue is more efficient in metal ion binding than the peptide without His (Fig. S11). This also additionally confirms that beside thiols, the imidazole nitrogen of His is involved in metal

ion coordination. It is interesting to note that the binding ability of both peptides lacking the His residue (ELES and DYGS) is almost the same, indicating that other residues have only a minor effect on the binding efficiency by thiol donors in equimolar complexes (Fig. 2). The presence of His in DYG and ELE peptides makes the N-terminal site where His and Cys residues are separated by Ser residue more efficient than the C-terminal one, where His is next to Cys residue (Fig. 3).

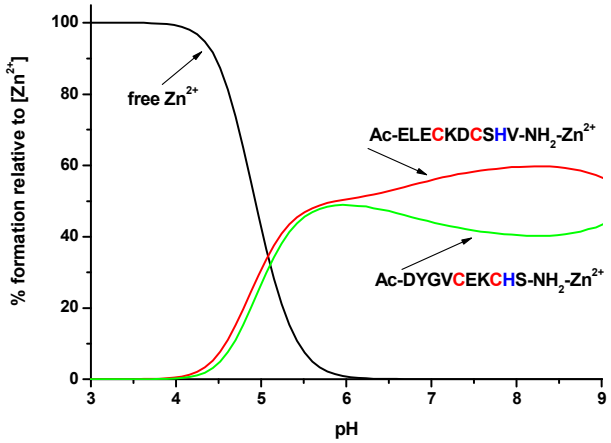

Fig. 3 A competition plot of Zn^{2+} complexes with ELE and DYG (1 : 1 : 1 molar ratio).

When the peptide to Zn^{2+} ratio is around 2, equimolar species were observed at lower pH, while above pH 7, bis-complexes dominate (Fig. S9). For peptides ELES and DYGS sulfurs from cysteine residues are the only donor atoms involved in the coordination to Zn^{2+} ion with {4S} binding mode (species ZnH_2L and ZnH_4L respectively). In the case of bis-complexes of the zinc ion with ELE, histidine residues participate in the coordination in the ZnH_4L_2 complex and the binding mode is {2S, $2N_{im}$}. As the pH increases, imidazole nitrogens are gradually replaced by cysteine thiols, thus in ZnH_2L_2, the binding mode is {4S}. Similar binding modes occur in the case of DYG peptide with Zn^{2+} ion.

Cd^{2+} complexes with ELE, ELES, DYG and DYGS peptides

Short peptides form both equimolar and bis-complexes also with Cd^{2+} (Tables 2-5; Fig. S12-S13). The coordination equilibria are similar to those observed for Zn^{2+}. The only difference is observed for DYG and DYGS peptides at lower pH, where the minor MH_3L species is present (Fig. S12). In the case of Cd^{2+} ions, a useful UV transition at 250 nm can be followed, which supports binding of metal ion to thiol sulfur. The intensity of this band is quite well related to the number of thiols bound to Cd^{2+}.[27-29] UV-VIS spectra of ELE-Cd^{2+} and DYG-Cd^{2+} indicate that at pH around 7.4, two thiols are bound to Cd^{2+}. In ^1H-^1H TOCSY spectra at pH 7.4 for these complexes, Hα–Hβ correlations from cysteine residues and correlations from aromatic protons of histidine residue are vanished compared to the spectra of free ligand at the same pH, which confirm the {2S, N_{im}} coordination mode as for Zn^{2+} species (Fig. S14-S15). Also in the case of Cd^{2+} ions, the stabilizing effect of the His residue is seen for both pairs of peptides (Fig. S16-S17). The much larger Cd^{2+} ion has different specificity towards both peptides than Zn^{2+}. DYG binds cadmium more efficiently than ELE (Fig. 4). Also comparison of ELES and DYGS shows some effect of adjacent residues on the stability of the formed complexes, making DYGS peptide more efficient in metal ion binding than ELES (Fig. 4).

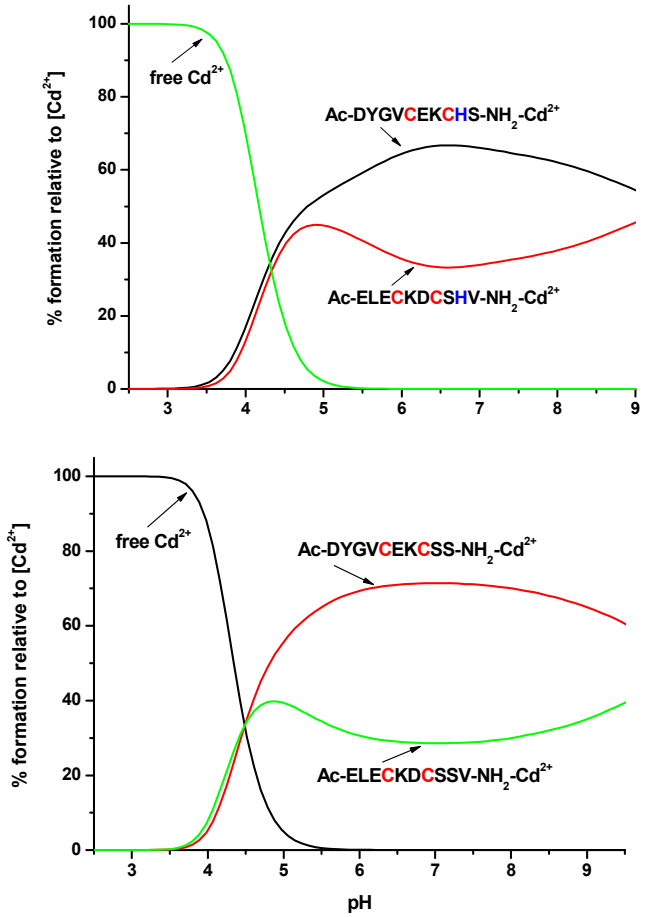

Fig 4 Competition plots of Cd^{2+} complexes with ELE and DYG (1 : 1 : 1 molar ratio).(top) and with ELES and DYGS (1 : 1 : 1 molar ratio) (bottom).

All shorter peptides form bis-complexes with Cd^{2+}. Four thiols from two peptide molecules are involved in the coordination to Cd^{2+}, which is clearly shown in the potentiometric and spectroscopic data (Tables 2-5; Fig. S13). The extinction coefficient at 250 nm for {4S} species is twice as high as the one observed for equimolar species with the {2S} coordination mode. As for Zn^{2+} complexes, equimolar species are also present in the solution at the lower pH, while at pH below 6, bis-complexes start to dominate. The presence of histidine, which may be close to Cd^{2+}, in the sequence of ELE and DYG, has a minor effect on the thermodynamic stability of cadmium complexes. In the case of ELE-Cd^{2+} and DYG-Cd^{2+} systems, the complex with the {4S} binding mode starts to form at

slightly higher pH (approximately 6) than in the case of ELES-Cd^{2+} and DYGS-Cd^{2+} (pH 5).

Ni^{2+} complexes with ELE, ELES, DYG and DYGS peptides

Peptides ELE, ELES, DYG and DYGS form only equimolar complexes with Ni^{2+} (Tables 2-5; Fig. S18). According to the calculations based on potentiometric data, there are four complexes of Ni^{2+} with ELE. NiHL dominates at pH 8 (Table 2; Fig. S18). The presence of the bands in the CD spectra at about 380 nm characteristic of S→Ni^{2+} charge transfer transitions support the involvement of thiol donors in the coordination.[29] The strong bands in the d-d region clearly show the formation of a planar complex. However, Hα–Hβ correlations of one of the cysteine residues (Cys-4) remain unaffected and the Hα–Hβ cross-peaks from the later one (Cys-7) are shifted after addition of Ni^{2+} into solution of the peptide in the ^{1}H-^{1}H TOCSY spectra. Additionally, shifting of aromatic protons signals of His imidazole ring from histidine are observed (Fig. 5). This indicates that both imidazole and amide nitrogens are involved in the coordination. NiL species results from the binding of the second amide nitrogen. The binding of the second amide donor is clearly seen in the distinct variation of the CD spectra (Fig. S19). The CD spectra do not change above pH 9 when deprotonations occur at second Cys and Lys residues. ELES also forms planar complexes, but at much higher pH with very different CD spectra, supporting the involvement of His residue from the ELE peptide in nickel binding (Fig. S20). This is also confirmed by the comparison of the binding ability of ELE and ELES - the ELE-Ni^{2+} complex is more stable (Fig. S21). In the case of Ni^{2+}-ELES system, the involvement of two thiols and two amide nitrogens in the formation of a planar complex is seen also in the ^{1}H-^{1}H TOCSY spectra, where Hα–Hβ correlations of cysteine residues are completely vanished (Fig. S22).

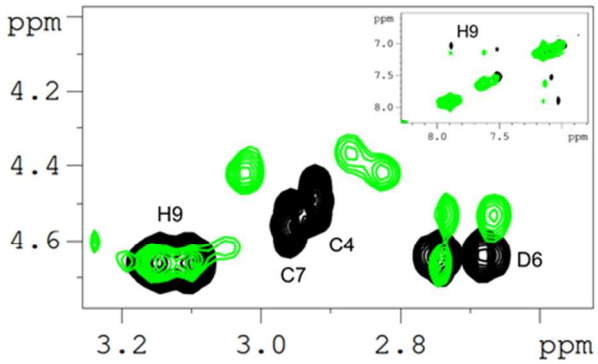

Fig. 5 Selected aliphatic regions of the ^{1}H–^{1}H TOCSY spectra of ELE at 1×10^{-3} M, pH 7.4 and T 303 K in the absence (black contours) and in the presence (green contours) of 0.7 Ni^{2+} equivalents.

Four DYG-Ni^{2+} complexes were detected in the measured pH range. NiHL, dominating at pH 8 (Table 4; Fig. S18), is the first complex of peptide DYG with Ni^{2+} that we are able to characterize. NiHL stoichiometry suggests the involvement of imidazole nitrogen, adjacent amide nitrogen and thiol of the vicinal Cys residue. This planar complex is the only one observed up to pH 10. Its coordination mode is confirmed by the presence of characteristic S→Ni^{2+} charge transfer bands in the CD spectra[29] (Fig. S23) and features of NMR spectra. In ^{1}H-^{1}H TOCSY spectra, Hα–Hβ correlations of one of the cysteine residue vanish with simultaneous appearance of new signals, while aromatic protons from imidazole ring of histidine are vanished (Fig. 6). DYGS also forms planar species above pH 7. The CD spectra differ considerably from those observed for Ni^{2+}-DYG system, supporting the finding that in the latter case His residue plays basic role in metal ion binding over a whole pH range (Fig. S24).

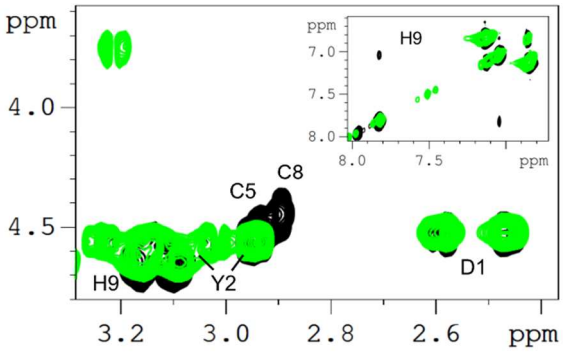

Fig. 6 Selected aliphatic regions of the ^{1}H–^{1}H TOCSY spectra of DYG at 1×10^{-3} M, pH 7.4 and T 303 K in the absence (black contours) and in the presence (green contours) of 0.7 Ni^{2+} equivalents.

Comparison of ELE-Ni^{2+} and DYG-Ni^{2+} shows that N-terminal motif (ELE) is more favorable than that on C-terminus (DYG) (Fig. 7).

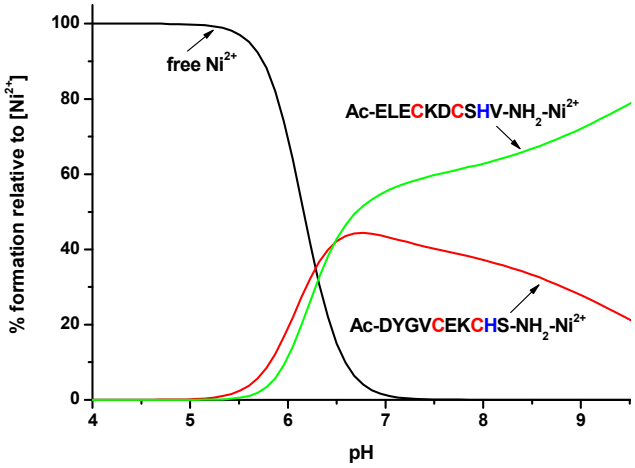

Fig. 7 A competition plot of Ni^{2+} complexes with ELE and DYG (1 : 1 : 1 molar ratio).

The role of the residues between two CXXC motifs in binding ability of HypA loop

Zn^{2+} complexes with HypA1, HypA2, HypA3 and HypA4

HypA1-HypA4 peptides form only equimolar complexes with Zn^{2+} (Tables 6-9; Fig. S25). In HypA1, the proline residue was replaced by alanine. In the case of HypA1-Zn^{2+} complexes,

Table 6 Potentiometric and spectroscopic data for proton, Zn^{2+}, Cd^{2+} and Ni^{2+} complexes of the HypA1 peptide.

			UV-Vis		CD	
Species	**log *β***	**p*K***	**λ/nm**	**ε/M^{-1} cm^{-1}**	**λ/nm**	**Δε/M^{-1} cm^{-1}**
HL	10.18 (4)	10.18 K				
H_2L	20.27 (1)	10.09 Y				
H_3L	29.71 (2)	9.44 C				
H_4L	38.54 (1)	8.83 C				
H_5L	46.94 (1)	8.40 C				
H_6L	54.04 (2)	7.10 C				
H_7L	60.36 (2)	6.32 H				
H_8L	65.42 (2)	5.06 H				
H_9L	69.68 (2)	4.26 E				
$H_{10}L$	73.55 (2)	3.87 E				
$H_{11}L$	76.95 (2)	3.40 E				
Zn^{2+} complexes						
ZnH_6L	59.51 (2)					
ZnH_4L	49.61 (2)					
ZnH_3L	43.49 (4)	6.12				
ZnH_2L	36.21 (4)	7.28				
ZnL	14.80 (4)					
Cd^{2+} complexes						
CdH_7L	65.62 (2)					
CdH_5L	57.10 (3)					
CdH_3L	47.09 (4)					
CdHL	34.59 (5)					
CdL	23.79 (7)	10.80				
Ni^{2+} complexes						
			276	5020	269	0.74
NiH_4L	46.33 (1)		297	4040	306	0.96
			342	2290	337	-0.35
					361	-0.47
					409	0.27
					508	0.48
					614	-0.33
NiH_3L	39.44 (3)	6.89	270	2850	261	1.24
			299	4070	312	0.66
			339	1660	362	-0.68
					496	1.15
					626	-0.35
NiH_2L	31.33 (4)	8.11	259	9330	260	1.90
			296	4120	276	1.60
			340	1600	317	0.43
			500	300	368	-1.23
					499	0.75
					637	-0.18
NiL	11.25 (4)		244	15910	250	2.48
			296	4860	270	2.70
			437	330	299	-0.23
					319	0.14
					361	-0.67
					469	0.33
					647	-0.11
$NiH_{-2}L$	-10.09 (4)		244	18645	258	2.86
			296	4665	299	-0.48
			436	250	303	-0.44
					364	-0.34
					409sh	-0.18
					462	0.37
					551sh	0.12

potentiometric data clearly show the participation of all cysteine residues in metal ion binding (Table 6; Fig S25). In the first calculated species, ZnH_6L, with a maximum concentration at pH 4.5, Zn^{2+} is bound by one cysteine thiol and one histidine

Table 7 Potentiometric and spectroscopic data for proton, Zn^{2+}, Cd^{2+} and Ni^{2+} complexes of the HypA2 peptide.

			UV-Vis		CD	
Species	**log *β***	**p*K***	**λ/nm**	**ε/M^{-1} cm^{-1}**	**λ/nm**	**Δε/M^{-1} cm^{-1}**
HL	10.14 (1)	10.14 K				
H_2L	20.18 (1)	10.04 Y				
H_3L	29.45 (1)	9.27 C				
H_4L	38.24 (1)	8.79 C				
H_5L	46.49 (1)	8.25 C				
H_6L	53.52 (1)	7.03 C				
H_7L	59.73 (1)	6.21 H				
H_8L	64.53 (1)	4.80 H				
H_9L	68.70 (1)	4.17 E				
$H_{10}L$	72.45 (1)	3.75 E				
$H_{11}L$	75.56 (1)	3.11 E				
Zn^{2+} complexes						
ZnH_5L	54.07 (2)					
ZnH_4L	48.86 (3)	5.21				
ZnH_3L	43.50 (3)	5.36				
ZnH_2L	36.27 (5)	7.23				
ZnL	15.88 (6)					
Cd^{2+} complexes						
CdH_7L	64.61 (3)					
CdH_5L	56.36 (3)					
CdH_3L	46.68 (4)					
CdHL	34.82 (6)					
CdL	24.04 (8)	10.78				
Ni^{2+} complexes						
NiH_4L	45.82 (1)		275	3724	300	0.86
			302	2410	360	-0.60
			345	1602	410	0.27
					510	0.30
					620	-0.21
NiH_3L	39.07 (1)	6.75	270	7847	310	0.67
			295	5080	360	-0.69
			344	2004	410	0.25
					500	0.36
					610	-0.29
NiH_2L	31.16 (2)	7.91	260	12111	320	0.16
			297	4916	360	-0.87
			342	1499	430sh	-0.04
			503	261	500	0.47
					630	-0.17
NiHL	21.41 (3)	9.75	248	16849	310	0.26
			344	1423	360	-0.71
			511	239	420	-0.23
					480	0.12
					620	-0.11
NiL	11.19 (2)	10.22	244	20080	314	0.18
			438	330	361	-0.51
					422	-0.21
					471	0.11
					540sh	0.04
					629	-0.08
$NiH_{-2}L$	-9.68 (2)		244	23310	311	0.26
			436	270	360	-0.70
					421	-0.23
					476	0.12
					537sh	0.06
					629	-0.12

Table 8 Potentiometric and spectroscopic data for proton, Zn^{2+}, Cd^{2+} and Ni^{2+} complexes of the HypA3 peptide.

			UV-Vis		CD	
Species	**log *β***	**p*K***	**λ/nm**	**ε/M^{-1} cm^{-1}**	**λ/nm**	**Δε/M^{-1} cm^{-1}**
HL	10.05 (2)	10.05 K				
H_2L	19.86 (1)	9.81 Y				
H_3L	28.87 (1)	9.01 C				
H_4L	37.51 (1)	8.64 C				
H_5L	45.29 (1)	7.78 C				
H_6L	52.00 (1)	6.71 C				
H_7L	57.90 (1)	5.90 H				
H_8L	62.31 (1)	4.41 H				
H_9L	66.67 (1)	4.36 E				
$H_{10}L$	70.14 (1)	3.47 E				
$H_{11}L$	73.59 (1)	3.45 E				
Zn^{2+} complexes						
ZnH_5L	53.94 (2)					
ZnH_3L	43.61 (2)					
ZnH_2L	36.65 (4)	6.96				
ZnL	15.63 (5)					
Cd^{2+} complexes						
CdH_8L	66.79 (1)					
CdH_6L	59.73 (5)					
CdH_4L	50.91 (8)					
CdH_3L	46.04 (8)	4.87				
CdHL	35.05 (9)					
CdL	24.1 (1)	10.95				
Ni^{2+} complexes						
NiH_4L	44.31 (1)		276	2720	267	0.06
			301	4210	298	0.15
					401	0.04
					505	0.04
NiH_3L	38.26 (1)	6.05	277	5585	265	2.73
			302	4190	306	3.06
			346	2480	351	-2.32
					401	0.64
					508	0.52
					607	-0.72
NiH_2L	31.06 (2)	7.20	273	6335	267	1.91
			301	3660	306	2.47
			346	1660	350	-1.70
			529sh	210	410	0.02
					503	1.35
					626	-0.54
NiHL	22.18 (3)	8.88	266	10890	262	3.24
			528sh	150	306	2.15
					360	-1.82
					413sh	0.14
					496	1.43
					620	-0.45
NiL	11.91 (3)	10.27	266	12110	258	3.76
			440	240	271	3.24
					309	1.27
					357	-1.57
					409sh	0.12
					493	1.03
					626	-0.33
$NiH_{-2}L$	-9.01 (3)		266	12610	247	4.05
			440	220	259	3.99
					272	3.49
					310	0.65
					355	-1.12
					469	0.60
					636	-0.21

Table 9 Potentiometric and spectroscopic data for proton, Zn^{2+}, Cd^{2+} and Ni^{2+} complexes of the HypA4 peptide.

			UV-Vis		CD	
Species	**log *β***	**p*K***	**λ/nm**	**ε/M^{-1} cm^{-1}**	**λ/nm**	**Δε/M^{-1} cm^{-1}**
HL	10.14 (1)	10.14 Y				
H_2L	19.85 (1)	9.71 C				
H_3L	28.78 (1)	8.93 C				
H_4L	37.35 (1)	8.57 C				
H_5L	45.18 (1)	7.83 C				
H_6L	51.53 (1)	6.35 H				
H_7L	56.30 (1)	4.77 E				
H_8L	60.53 (1)	4.23 E				
H_9L	64.33 (1)	3.80 E				
$H_{10}L$	67.53 (1)	3.20 D				
Zn^{2+} complexes						
ZnH_4L	45.91 (3)					
ZnH_3L	40.62 (6)	5.29				
ZnH_2L	34.83 (6)	5.79				
ZnHL	27.73 (7)	7.10				
ZnL	17.60 (8)	10.13				
Cd^{2+} complexes						
CdH_8L	65.89 (3)					
CdH_6L	58.83 (4)					
CdH_4L	51.14 (5)					
CdH_3L	46.25 (9)	4.89				
CdH_2L	41.16 (8)	5.09				
CdHL	35.35 (8)	5.81				
CdL	24.4 (1)	10.95				
Ni^{2+} complexes						
NiH_3L	37.86 (1)		301	7110	263	3.66
			347	4370	289	-0.74
			424	1380	308	4.53
			536	420	350	-3.55
					395	1.18
					457	-0.64
					504	-0.27
					595	-1.30
NiH_2L	30.76 (2)	7.10	268	10020	264	8.28
			301	11310	289	0.60
			346	6820	308	9.64
			530	660	350	-7.45
					396	2.23
					454	-0.63
					502	0.42
					603	-2.47
NiHL	21.56 (3)	9.20	264	11390	263	8.89
			300	10470	289	0.52
			346	6260	308	10.28
			530	610	350	-7.97
					400	2.27
					456	-0.63
					504	0.49
					598	-2.21
NiL	11.14 (3)	10.42	minor			
$NiH_{-2}L$	-10.38 (5)		262	12510	263	8.44
			297	9730	289	0.27
			346	5840	308	9.48
			530	570	350	-7.67
					398	1.97
					456	-0.89
					503	0.22
					598	-2.45

imidazole. Next two deprotonations from the second imidazole group and the second thiol lead to ZnH_4L species, with the

maximum at pH about 5.5, where a {2N_{im}, 2S} coordination mode is observed. In ZnH_3L complex, one imidazole group from histidine residue is substituted by another thiol group. In the ZnH_2L, a four coordinated complex with {4S} binding mode can be detected. The last two deprotonations belong to tyrosine and lysine residues which do not take part in binding. Described above, interesting pH-dependent His-Cys binding switch mechanism is observed also for WT HypA.[19]

In HypA2 and HypA3 derivatives (Table 7-8; Fig. S25), one can observe Zn^{2+} complexes with similar binding modes, since the main difference between them is the length of the linker between CXXC motifs. Two thiols and two imidazole groups are involved in the coordination at lower pH, while at pH above 7.4, the mode of the binding changes to four thiols {4S}, which is visible in NMR. In ^{1}H-^{1}H TOCSY spectra of HypA3 at pH 6.4, one can clearly notice the shift of Hα-Hβ correlations of cysteine and histidine residues, but also proton correlations belonging to imidazole protons are broadened (Fig. 8). At pH around 8, when the spectra of free ligand and Zn^{2+} complex are compared, one can find that Hα–Hβ cross-peaks from protons belonging to side chains of cysteine residues are shifted, whereas those from histidine are only slightly affected (Fig. 8).

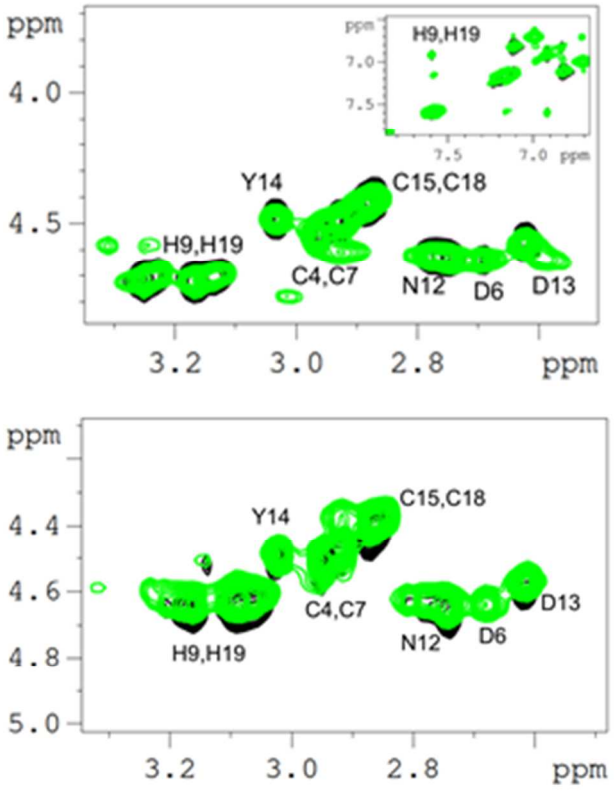

Fig. 8 Selected aliphatic and aromatic regions of the ^{1}H–^{1}H TOCSY spectra of HypA3 at 1×10^{-3} M, pH 6.4 (top), pH 8.0 (bottom) and T 303 K in the absence (black contours) and in the presence (green contours) of 0.5 Zn^{2+} equivalents.

Lack of one of histidine and shorter linker between CXXC motifs in HypA4 causes that in species present at pH 6.4, the binding mode is {3S, N_{im}} (Table 9; Fig. S18). However, as for peptides described above this coordination changes to {4S} at pH 8, which is confirmed by NMR spectra (Fig. 9).

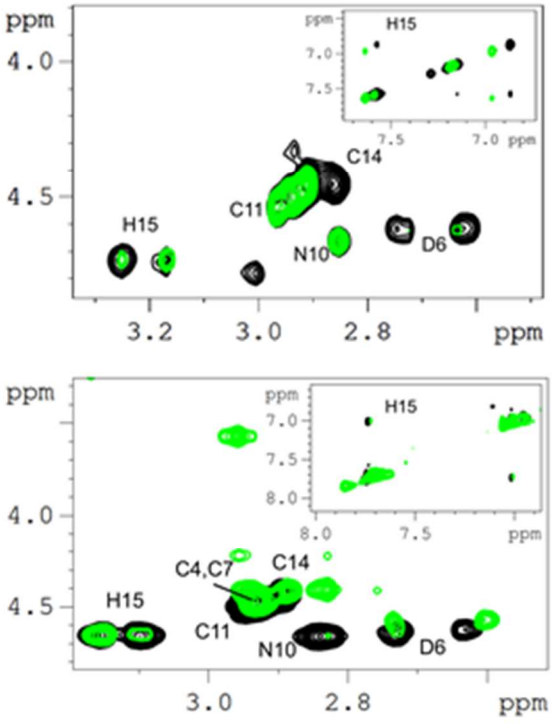

Fig. 9 Selected aliphatic and aromatic regions of the ^{1}H–^{1}H TOCSY spectra of HypA4 at 1×10^{-3} M, pH 6.4 (top), pH 8.0 (bottom) and T 303 K in the absence (black contours) and in the presence (green contours) of 0.5 Zn^{2+} equivalents.

Cd^{2+} complexes with HypA WT, HypA1, HypA2, HypA3 and HypA4

HypA WT peptide, as well as its derivatives, form equimolar complexes with Cd^{2+} (Tables 6-10; Fig. S26-S27). The binding modes of these complexes are very similar to those observed for Zn^{2+} with thiol and imidazole groups as anchoring sites at lower pH and only the thiol groups involved in the binding at higher pH (above 6). The stability constants for Cd^{2+} complexes are distinctly higher than those of Zn^{2+} and the first cadmium species are observed at lower pH (about 3) than in the case of zinc (pH>4). Accurate assignment of the binding groups for the corresponding complexes formed at lower pH range is rather difficult because of the overlapping of the complex species. However, the increase of the extinction coefficient for the transition at 250 nm confirms the involvement of consecutive thiol groups in the metal ion binding (Fig. S28). In CdH_3L species for HypA WT, HypA1, HypA2 and HypA3 and CdH_2L for HypA4-Cd^{2+} the coordination involves the {3S, N_{im}} donor set, which is indicated by ^{1}H-^{1}H TOCSY spectra of HypA3 and Hypa4 at pH 6.4 (Fig. S29-S30). The shifting of Hα-Hβ correlations of cysteine and histidine residues are observed. The binding mode for the following complex is {4S}. This coordination mode is confirmed by UV-VIS and NMR spectra. In ^{1}H-^{1}H TOCSY spectra of HypA3 and HypA4 at pH 8 only Hα-Hβ correlations of cysteine residues are shifted and these

belonging to histidine residues remain unaffected (Fig. S29-S30).

Table 10 Potentiometric and spectroscopic data for proton and Cd^{2+} complexes of the HypA WT peptide.

Species	log *β*	p*K*	
HL	10.81 (1)	10.81	K
H_2L	21.20 (1)	10.39	Y
H_3L	30.92 (1)	9.72	C
H_4L	39.82 (1)	8.90	C
H_5L	48.09 (1)	8.27	C
H_6L	55.06 (1)	6.97	C
H_7L	61.22 (1)	6.16	H
H_8L	65.97 (1)	5.06	H
H_9L	70.16 (1)	4.19	E
$H_{10}L$	73.99 (1)	3.83	E
$H_{11}L$	76.97 (1)	2.98	E
Cd^{2+} complexes			
CdH_7L	65.98 (2)		
CdH_5L	57.53 (2)		
CdH_3L	47.16 (3)		
CdHL	33.39 (4)		
CdL	23.47 (5)	9.92	

Ni^{2+} complexes with HypA1, HypA2, HypA3 and HypA4

According to calculations based on potentiometric data, in the studied pH range there are five Ni^{2+}complexes with HypA1. The intense band at about 280 nm in the UV-VIS spectra observed for NiH_4L species is most likely composed of a mixture of $N_{im}\rightarrow Ni^{2+}$ and $S\rightarrow Ni^{2+}$ charge transfer transitions,[30-32] suggests that histidine imidazoles and cysteine thiols are involved in the coordination (Table 6, Fig. S31). Distinct changes in the CD spectra observed for NiH_3L suggest that the first amide nitrogen is bound to Ni^{2+},[19] while in NiL species the second amide nitrogen participates in the binding to Ni^{2+} (Fig. S32). In the latter case, there is a distinct shift of the band from 498 to 469 nm. Also in UV-VIS spectra, the d-d band at about 440 nm is observed, confirming planar geometry of the Ni^{2+} complexes.[33] Lack of changes in spectroscopic data for the next two species indicates that they arise from the deprotonation of tyrosine or lysine residues which are not coordinated to metal ion.

The UV-VIS and CD spectra are almost identical with those observed for Ni^{2+} complexes with Ac-ELECKDCSHVFKPNALDYGVCEKCHS-NH_2 peptide (HypA WT).[19] This suggests that the same donor atoms are coordinated to nickel ion as in case of nickel complex with that fragment of the HypA loop: the sulfur atom from Cys-7, backbone amide nitrogens of Ser-8 and His-9 and the imidazole nitrogen from His-9. In the case of HypA2 and HypA3 peptides, the decreasing number of residues between CXXC motifs does not affect the mode of the coordination for NiL species. We also observe the formation of the square planar nickel complex with residues on the N-terminal site. It is supported by potentiometric and spectroscopic data (Tables 7, 8; Fig. 10; Fig. S31, S33).

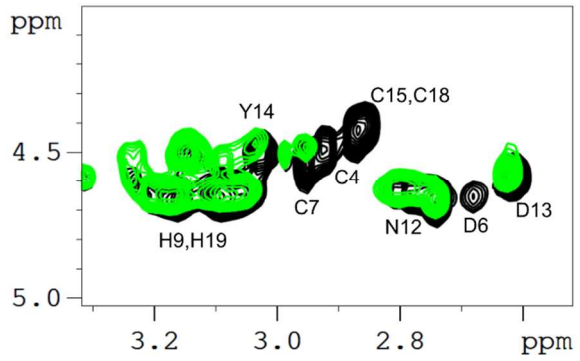

Fig. 10 Selected aliphatic regions of the $^1H–^1H$ TOCSY spectra of HypA3 at 1×10^{-3} M, pH 8.0 and T 303 K in the absence (black contours) and in the presence (green contours) of 0.5 Ni^{2+} equivalents.

In case of HypA4 the situation is different. The absence of the crucial histidine residue in the motif on the N-terminal site and shorter linker between CXXC motifs has a significant influence on Ni^{2+} coordination. The mode of the coordination is {2S, $2N_{amide}$} for $NiH_{-2}L$ species. It is confirmed by presence of an intense $S\rightarrow Ni^{2+}$ charge transfer bands at about 310 and 350 nm, and the d-d bands in the CD spectra (Fig. S34).[29] Also in ^1H-^1H TOCSY spectra of HypA4-Ni^{2+} Hα–Hβ cross-peaks from some of cysteine residues are vanished at pH 8 (Fig. 11). According to CD spectra, this species starts to form above pH 6. It could suggest that the same coordination mode as in the latter complex occurs also for NiH_2L, NiHL and NiL species as well.

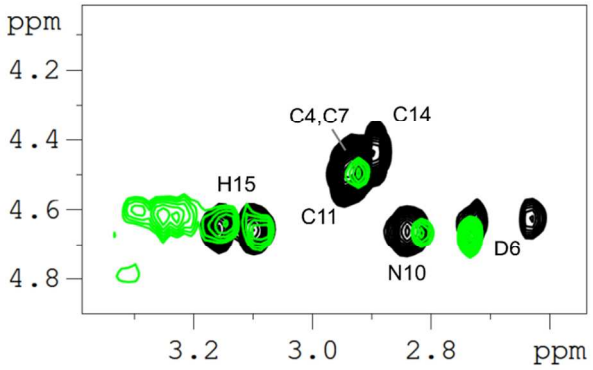

Fig. 11 Selected aliphatic regions of the $^1H–^1H$ TOCSY spectra of HypA4 at 1×10^{-3} M, pH 8.0 and T 303 K in the absence (black contours) and in the presence (green contours) of 0.5 Ni^{2+} equivalents.

Comparison of the complexation abilities of the peptides containing two CXXC motifs towards Zn^{2+} and Cd^{2+} ions

The most intriguing question was whether the lack of proline residue can change the thermodynamic stability of the studied complexes. A competition plot between zinc species with the fragment of HypA loop and Zn^{2+} complexes with HypA1 peptide clearly shows that the lack of proline residue significantly increases the stability of the Zn^{2+} complexes (Fig. 12A). The same is true for Cd^{2+} complexes with HypA WT and HypA1 peptides (Fig. 12B).

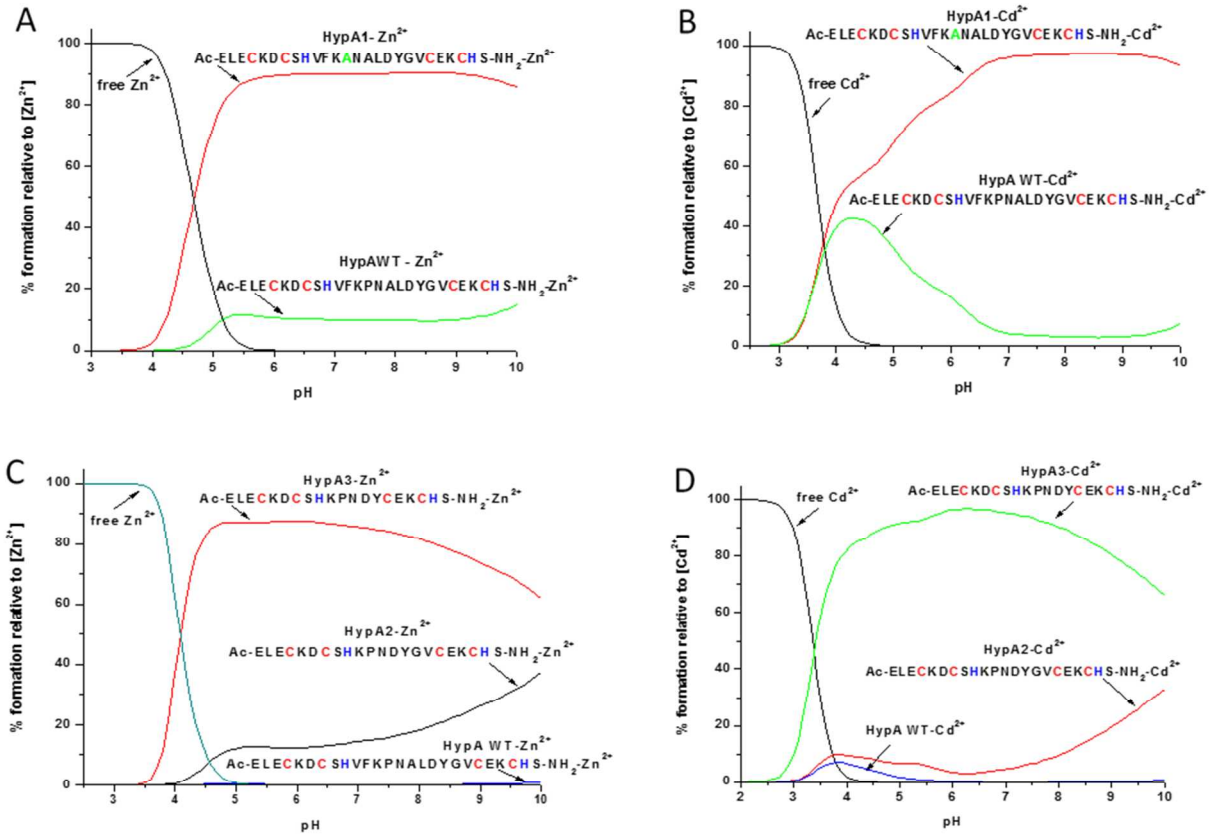

Fig. 12 Competition plots of Zn^{2+} (A) and Cd^{2+} (B) complexes with HypA WT and HypA1 (1 : 1 : 1 molar ratios) and Zn^{2+} (C) and Cd^{2+} (D) complexes with HypA WT, HypA2 and HypA3 (1 : 1 : 1 : 1 molar ratios).

Probably the lack of proline residue leads to a higher flexibility of the peptide chain and stabilization of the formed complexes.

The aim of the other modifications of HypA loop sequence was to check how the length and sequence of the linker between CXXC motifs influences the stability of the investigated complexes. In the case of Zn^{2+} and Cd^{2+} complexes, the HypA2 derivative ($CXXC(X)_9CXXC$) is a more effective ligand than HypA WT ($CXXC(X)_{13}CXXC$). Further reduction of the distance between CXXC motifs (HypA3 - $CXXC(X)_7CXXC$) results in further increase stability of Zn^{2+} and Cd^{2+} complexes when compared to HypA WT species (Fig. 12C,12D).

Conclusions

The loop domain of HypA comprise two effective metal ion binding sites consisting of pairs of cysteinyl thiols, accompanied by His imidazoles adjacent to each of the CXXC motifs. In the case of Zn^{2+} ions more effective is imidazole of His separated from Cys pair by Ser residue (N-terminal site) when compared to His being next to Cys pair (C-terminal site). When His residues were mutated with Ser both thiol binding sites show very similar coordination ability. Situation is different for Cd^{2+}, where peptide with C-terminal motif has better binding ability than that with N-terminal, regardless of whether His is in the sequence or not. It can be explained by some effect of adjacent residues on the stability of the formed complexes.

In the case of Ni^{2+} binding mode is different than for Zn^{2+} and Cd^{2+}. Only one Cys of CXXC motif is involvement in the binding, and the coordination sphere is completed with imidazole and amide nitrogens. The N-terminal site is much more favorable than the C-terminus.

The results obtained for the long fragments of the loop domain both for Zn^{2+} and Cd^{2+} ions clearly indicate the distinct role of Pro residue situated in the central part of the loop. Its presence strongly decreases the binding efficacy what is essential in the variation of thiol sulfurs to imidazole nitrogen when pH decreases below pH 7. It was also shown that length of the linker between two thiol sites has very distinct impact on the coordination ability.

Acknowledgements

P. R. Chetana sincerely thank Indian National Science Academy-Polish Academy of Sciences, New Delhi, India for providing Bilateral Exchange of Scientists Fellowship.

Notes and references

[a] Faculty of Chemistry, University of Wroclaw, 14 F. Joliot-Curie St., Wroclaw, Poland.
E-mail: henryk.kozlowski@chem.uni.wroc.pl; Fax: +48 71 375 72 51;
Tel: +48 71 375 72 51.
[b] Department of Chemistry, Central College Campus, Bangalore University, Bengaluru 560001, India.
[c] Faculty of Chemistry, University of Gdansk, 18 Sobieskiego St., Gdansk, Poland.

† Electronic Supplementary Information (ESI) available. See DOI: 10.1039/b000000x/

1 M. J. Blaser, P. H. Chyou and A. Nomura, *Cancer Res*., 1995, **55**, 562-565.
2 World Health Organisation, "Schistosomes, liver flukes and Helicobacter pylori. IARCWorking Group on the Evaluation of Carcinogenic Risks to Humans. Lyon, 7–14 June 1994," IARC Monographs on the Evaluation of Carcinogenic Risks to Humans / World Health Organization, International Agency for Research on Cancer, vol. **61**, pp. 1–241, 1994.
3 H. M. Malaty*, Best Pract. Res. Cl. Ga*., 2007, **21**, 205.
4 D. R. Scott, E. A. Marcus, D. L. Weeks and G. Sachs, *Gastroenterology*, 2002, **123**, 187.
5 J. W. Olson and R. J. Maier, *Science*, 2002, **298**, 1788.
6 R. J. Maier, S. L. Benoit and S. Seshadri, *BioMetals*, 2007, **20**, 655.
7 S. B. Mulrooney and R. P. Hausinger, *FEMS Microbiol. Rev*., 2003, **27**, 239.
8 H. Kaluarachchi, K. C. Chan Chung and D. B. Zamble, *Nat. Prod. Rep*., 2010, **27**, 681.
9 D. Witkowska, M. Rowinska-Zyrek, G. Valensin and H. Kozlowski, *Coord. Chem. Rev*., 2012, **256**, 133.
10 M. Rowinska-Zyrek, J. Zakrzewska-Czerwinska, A. Zawilak-Pawlik and H. Kozlowski, *Dalton Trans*., 2014, **43**, 8976.
11 J. W. Olson, N. S. Mehta and R. J. Maier, *Mol. Microbiol.*, 2001, **39**, 176.
12 W. Xia, H. Li, X. Yang, K.-B. Wong and H. Sun, *J. Biol. Chem*., 2012, **287**, 6753..
13 C. D. Douglas, T. T. Ngu, H. Kaluarachchi and D. B. Zamble, *Biochemistry*, 2013, **52**, 6030.
14 S. Watanabe, T. Arai, R. Matsumi, H. Atomi, T. Imanaka and K. Miki, *J. Mol. Biol*., 2009, **394**, 448.
15 M. Blokesch, M. Rohrmoser, S. Rode and A. Bock, *J. Bacteriol*., 2004, **186**, 2603.
16 W. Xia, H. Li, K.-H. Sze and H. Sun, *J. Am. Chem. Soc*. 2009, **131**, 10031.
17 D. C. Kennedy, R. W. Herbst, J. S. Iwig, P. T. Chivers and M. J. Maroney, *J. Am. Chem. Soc*., 2007, **129**, 16.
18 R. W. Herbst, I. Perovic, V. Martin-Diaconescu, K. O'Brien, P. T. Chivers, S. S. Pochapsky, T. C. Pochapsky and M. J. Maroney, *J. Am. Chem. Soc*., 2010, **132**, 10338.
19 M. Rowinska-Zyrek, S. Potocki, D. Witkowska, D. Valensin and H. Kozlowski, Dalton Trans., 2013, 42, 6012- 6020.
20 G. Vanhoof, F. Goossens, I. De Meester, D. Hendriks and S Scharpé, *The FASEB Journal*, 1995, **9**, 736.
21 Atherton E, Sheppard RC. 1989. Solid Phase Peptide Synthesis: A Practical Approach. Oxford University Press: USA.
22 G. B. Fields and R. L. Noble, *Int. J. Pept. Protein Res.*, 1990, **35**, 161.
23 H. Irving, M. Miles and L. Pettit, *Anal. Chim. Acta*, 1967, **38**, 475.
24 G. Gran, *Acta Chem. Scand*., 1950, **4**, 559.
25 P. Gans, A. Sabatini and A. Vacca, *J. Chem. Soc., Dalton Trans*., 1985, 1195.
26 P. Gans, A. Sabatini and A. Vacca, *Talanta*, 1996, **43**, 1739.
27 P. Kuan-yeu Pan, Z. F. Zheng, P. C. Lyu and P. C. Huang, *Eur. J. Biochem*., 1999, **266**, 33.
28 P. Faller, D. W. Hasler, O. Zerbe, S. Klauser, D. R. Winge and M. Vasak*, Biochemistry*, 1999, **38**, 10158.
29 K. Kulon, D. Wozniak, K. Wegner, Z. Grzonka and H. Kozlowski, *J. Inorg. Biochem*., 2007, **101**, 1699.
30 K. Kulon, D. Valensin, W. Kamysz, R. Nadolny, E. Gaggelli, G. Valensin and H. Kozłowski, *Dalton Trans*., 2008, 5323.
31 P. Mlynarz, D. Valensin, K. Kociolek, J. Zabrocki, J. Olejnik and H. Kozlowski, *New J. Chem*., 2002, **26**, 264.
32 W. Bal, M. Jezowska-Bojczuk and K. S. Kasprzak, *Chem.Res. Toxicol*., 1997, **10**, 906.
33 M. Rowinska-Zyrek, D. Witkowska, D. Valensin, W. Kamysz and H. Kozłowski, *Dalton Trans*., 2010, **39**, 5814.

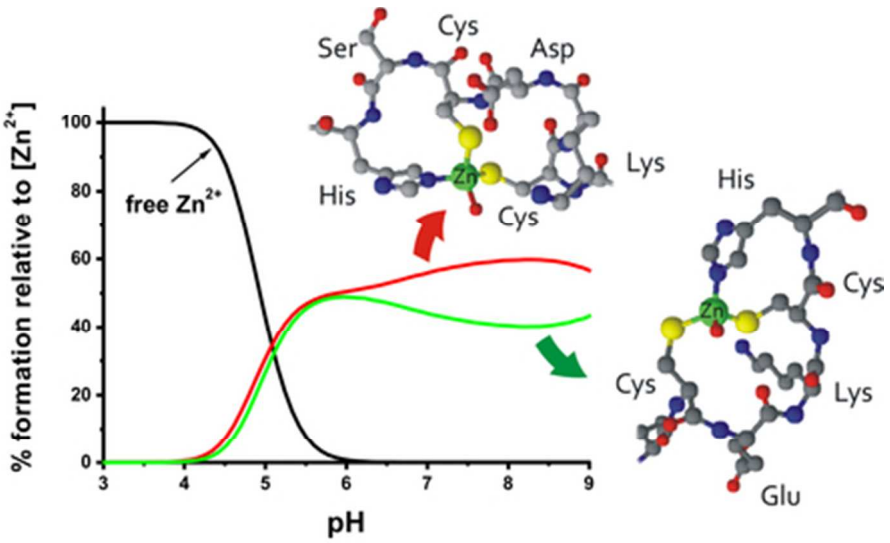

The role of the residues in the HypA loop on the stability of its complexes with Zn2+, Cd2+ and Ni2+ ions.
38x22mm (300 x 300 DPI)